Tracking the evolution of hot tears in aluminium alloys using high-speed X-ray imaging

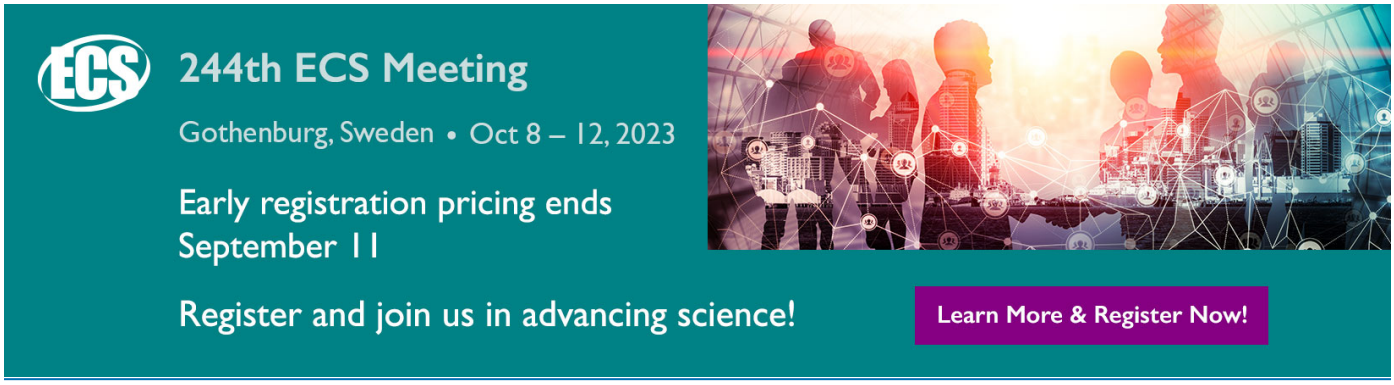

Tracking the evolution of hot tears in aluminium alloys using high-speed X-ray imaging

Insung Han[1], Shikang Feng[1], Andrew Lui[1], Fabian Wilde[2], Patrick S Grant[1] and Enzo Liotti[1]*

[1]Department of Materials, University of Oxford, Oxford OX1 3PH, United Kingdom
[2]Institute of Materials Research, Helmholtz-Zentrum Hereon, Max-Planck-Straße 1, 21502 Geesthacht, Germany

E-mail: enzo.liotti@materials.ox.ac.uk

Abstract. Hot tears are detrimental defects forming during the final stage of solidification when the remaining liquid loses the capacity to compensate for liquid to solid volume shrinkage. Although a mature semi-quantitative description of hot tearing has been developed, little is known about the dynamic evolution of hot tears as experimental studies have been conducted mostly post-solidification or in semi-static *in-situ* conditions. Here, we present a methodology to investigate the evolution of hot tears with high spatial and temporal resolution using synchrotron-based X-ray radiography. We develop a novel hot tear detection and tracking algorithm for quantification of hot tear density, area fraction and merging from the analysis of radiographic sequences of the solidification of thin metal samples. The methodology is demonstrated for an Al-5wt%Cu alloy and examples of the results and new insights that can be achieved are described.

1. Introduction

Hot tearing is a shrinkage-induced defect often observed during the last stage of solidification and caused by the pressure drop due to a lack of liquid feeding of solidification shrinkage in the mushy zone [1]. Hot tears significantly degrade the mechanical properties of casting alloys, as they act as stress concentrators that encourage the formation and propagation of cracks [2]. So far, due to the technical difficulties in observing the propagation of hot tears in real time within opaque metal alloys, most of the experimental work on hot tearing has been conducted *ex-situ* [3–5], with relatively few *in-situ* studies [6–9]. Early *in-situ* approaches were based on transparent organic alloys, such as succinonitrile-acetone, to replicate dendritic structures equivalent to those found in metallic alloys [6]. However, thanks to the advancement of synchrotron technologies in the last 15 years, *in-situ* X-ray imaging techniques have been increasingly employed for the study of solidification phenomena in metallic materials, including hot tearing. Puncreobutr et al. [9] investigated the effects of intermetallic phases on liquid permeability of the interdendritic channel, which influenced the pressure drop evolution in the liquid within the mush, using time-resolved tomography. Sistaninia et al. [8] combined a 3D granular modeling and *in-situ* X-ray tomography to study crack propagation during tensile deformation in the semi-solid microstructure as a model of the mushy zone at high solid fraction. In this paper we present a novel methodology for capturing the onset of hot tears formation and their subsequent

growth and merging in an Al-5wt%Cu alloy using fast (up to 100 Hz) synchrotron-based X-ray radiography and advanced computer vision techniques.

2. Experimental methods

2.1. In situ solidification experiment

Radiographic videos of the solidification of grain refined Al-5wt%Cu samples were collected at the P05 beamline at the Petra III synchrotron (Germany) using our bespoke Bridgman furnace [10]. The furnace comprises two small ceramic plate heaters, which are independently controlled, enclosed in a chamber with Ar atmosphere. The arrangement of the rig in the beamline and the configuration of the heating plates are shown in figure 1. The experiments were carried out in near isothermal conditions by setting the same temperature for both heaters during cooling. In each sequence, thin alloy samples were melted and homogenised at 690 °C and then cooled at a constant cooling rate to a temperature of 510 °C, acquiring images at a variable rate to maintain a constant temperature step of 0.04 °C/frame. Cooling rates ranged from 0.5 °C/s to 4 °C/s and the corresponding acquisition rates from 12.5 Hz to 100 Hz respectively. A 19 keV monochromatic beam illuminated the alloy samples and the transmitted signal collected using a 200 µm LuAG:Ce screen combined with either a Ximea CB500MG or a KIT CMOS cameras. The field of view ranged between 4.51 mm × 3.38 mm and 6.55 mm × 4.92 mm with spatial resolutions of 1.1 µm/pixel and 1.3 µm/pixel. A large number of videos sequences were collected and we present illustrative examples of some of the key features to demonstrate the technique and analysis method.

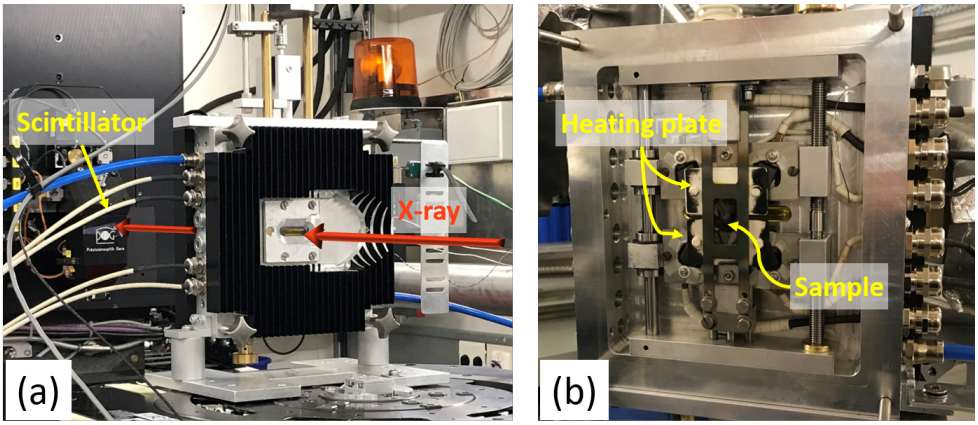

Figure 1. (a) Bridgman furnace setup at P05 beamline (Petra III). (b) The inside of the chamber showing the arrangement of the heating plates and sample.

2.2. Sample preparation

Alloys with composition Al-5wt%Cu were prepared using high purity Al (99.999%) and Al-80Cu master alloys. 0.1 wt% of Al-5Ti-1B and 1 wt% of pure Pb (99.999%) were also added for grain refinement and to form a fine emulsion of micron-scale Pb droplets to be used as flow tracers in the radiographic videos. Bulk samples were melted at 750 °C and homogenized for 10 minutes in an induction furnace under an Ar atmosphere. The molten metal was then poured into a water-cooled Cu mold. The small solid ingot was sectioned, ground and polished into thin foils with dimensions of 10 mm (width) × 20 mm (height) × 0.2 mm (thickness) for the synchrotron radiography experiments.

3. Hot tear detection and tracking

3.1. Algorithm

An algorithm was written in MATLAB language to detect hot tears as they appeared in the radiographic images, track their growth and characterise their merging behaviour. The algorithm is composed of two separated steps: in the first step the frames are analysed to detect all the hot tearing regions; in the second step the segmented images are further analysed to track the temporal evolution of each individual hot tear and any hot tears interactions such as merging.

3.1.1. Hot tear detection

Hot tears appeared as bright regions in the radiographs due to their low X-ray absorption compared with the surrounding liquid or solid metal. Hot tear appearance is demonstrated in Figs. 2(a-b) showing two sequential frames of a region of interest (ROI) in which a hot tear formed. In the detection algorithm, hot tears were detected by segmenting a difference image, which was obtained by subtracting the previous frame from the current frame. Image subtraction was needed to enhance the contrast between hot tears and the liquid in the interdendritic channels. The subtracted image was further processed to minimize the noise signal and then the obtained image was segmented using an intensity-based thresholding approach. Figure 2(c) shows the results of the segmentation procedure applied to the ROI in figure 2(a-b).

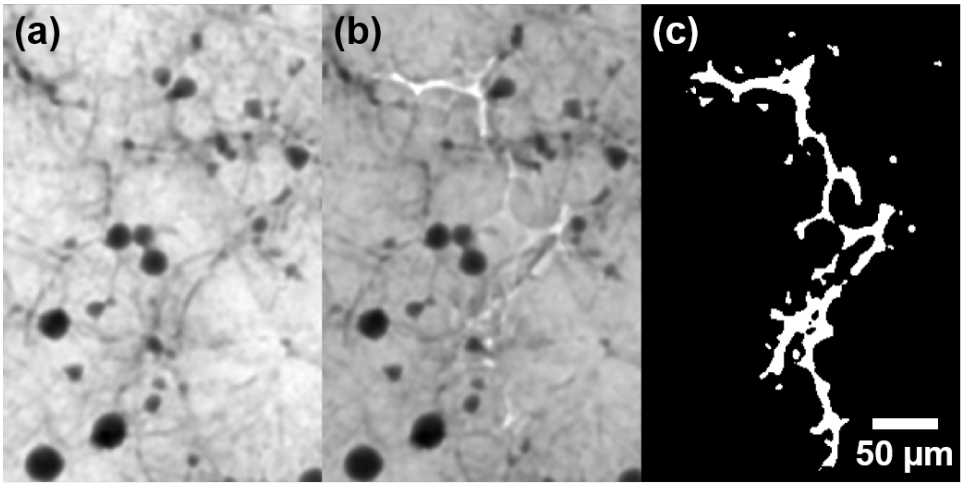

Figure 2. (a, b) Consecutive radiography images, at time t, prior to hot tearing and at t + 0.02 s, after hot tearing, respectively. (c) A hot tear identified by subtracting image (a) from image (b), followed by appropriate thresholding.

3.1.2. Unique identifiers for hot tear tracking

The segmented images were further processed by applying a dilation morphological operation with a 10 pixel × 10 pixel structuring element to all the foreground objects. This operation was needed to correctly identify each hot tear in the segmented images. Without the dilation routine, the hot tears often appeared fragmented into smaller pieces only because of limitations in spatial resolution and blurring. An example of this operation is shown in figure 3(a). The white pixels represent the hot tearing region detected by segmentation. By applying dilatation, only two unconnected regions remain (in blue and red) and these were assigned a unique identifier (UI). For each UI, detailed information, such as hot tear size, location and formation temperature, was recorded every frame from the first detection. As hot tears were spatially fixed, frame to

frame UI matching was achieved simply by testing if each new detection included an existing hot tear. When there was overlap between dilated hot tears with different UIs, a merging event was assumed, a new UI was assigned to the merged tear, and the prior hot tears no longer tracked. Instead, the newly merged hot tear was tracked. An example is shown in figure 3(b) where the dilated hot tear (magenta color) now contained the information associated with the pre-formed hot tears in figure 3(a).

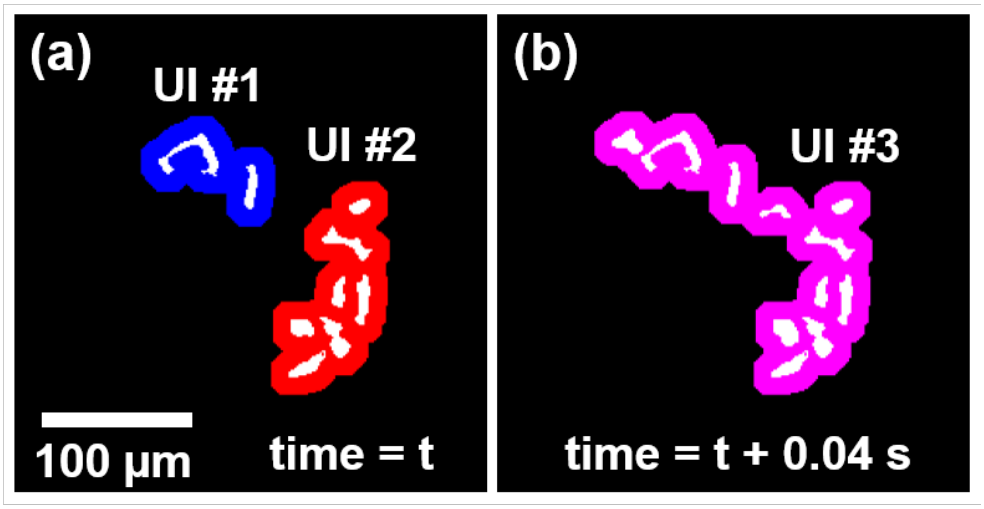

Figure 3. (a) Segmented hot tears (white pixels) with their own UIs (blue and red pixels). (b) A merged hot tear from the pre-formed hot tears in (a), with a newly assigned UI (magenta pixels).

3.2. Application: hot tear formation and growth analysis

Figures 4(a)-(d) are a typical image sequence from the late stage of the solidification of Al-5wt%Cu cooled at $2\,^{\circ}\mathrm{C\,s^{-1}}$ showing the formation of hot tears. The instantaneous temperature in each image was determined by knowing the temperature and frame at which primary α-Al dendrites in Al-5wt%Cu were first detected (liquidus temperature = 647.2 °C) and then recalculating the temperature of each subsequent frame according to the cooling rate and time elapsed since the first dendrite was observed. Using the Al-Cu phase diagram, the solid fraction was estimated as 0.88 and the average Al grain size was ≈200 µm. The black Pb droplets in figure 4, formed by monotectic reaction in the early stage of solidification and were located and entrained within the interdendritic channels. The Pb droplets were also tracked to help characterise the liquid flow in the last stage of solidification, as described in [11]. Hot tears, highlighted in cyan for clarity, first appeared at a temperature of 552.5 °C, and increased in number thereafter. Although hot tears formed across the entire FOV, they were, in this case, clustered in the bottom left region of figure 4(d).

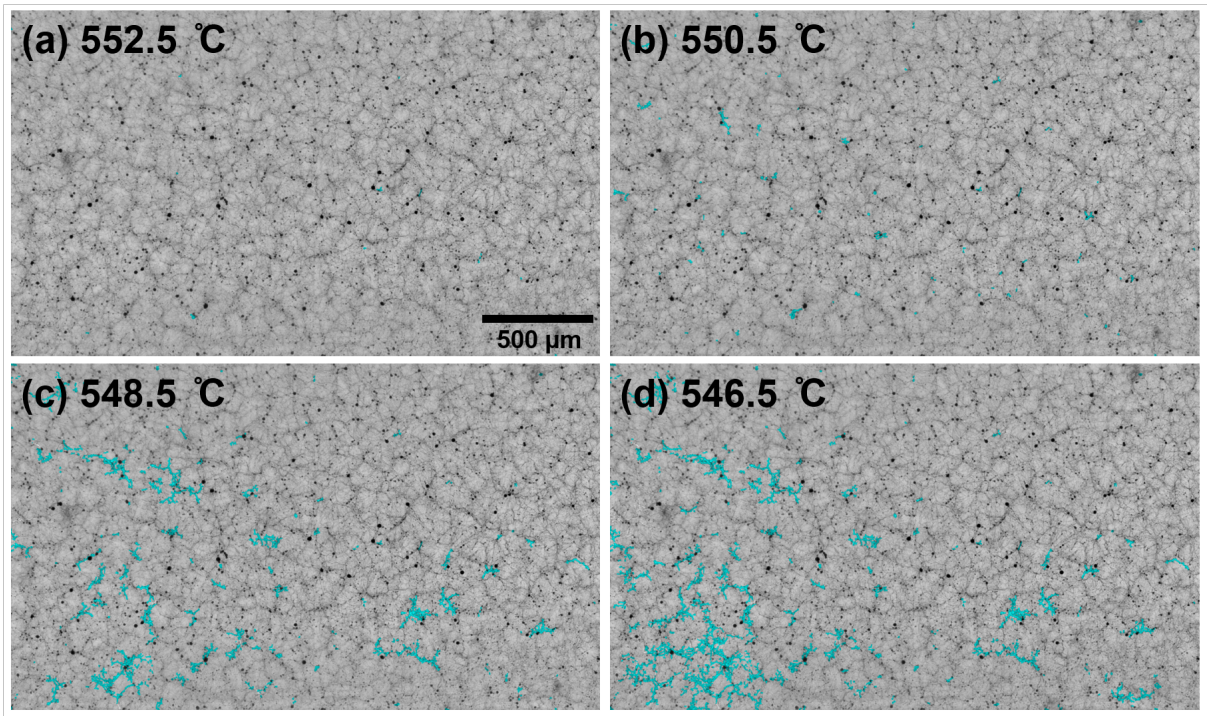

Figure 4. Sequence of radiographs of the solidification of Al-5wt%Cu cooled at 2 °C s^{-1} showing the microstructure at increasing solid fraction in the last stages of solidification. Hot tears are highlighted in cyan (and are dilated for visualization purposes). Pb droplets (black) flowing in the interdendritic regions are also visible.

The hot tear density was determined by counting the number of active hot tears (i.e. with separeate UIs) per unit area in each frame and is plotted in figure 5 (blue curve). The hot tear density increased steadily up to 10 hot tear/mm^2, and then plateaued. The occasional slight reductions in hot tear density in figure 5 below 549 °C were attributed to the merging of hot tears. The overall hot tear area fraction was calculated by summing the white pixels within the field of view in each frame and is the orange curve in figure 5. The curve follows the trend of the hot tear density, but delayed in time indicating that in the early stage of hot tear formation, growth was primarily due to nucleation of new hot tears, whereas the later stage was primarily due to growth. Both curves had an approximate Avrami *S-shape*, typical of classical nucleation and growth phase transformations.

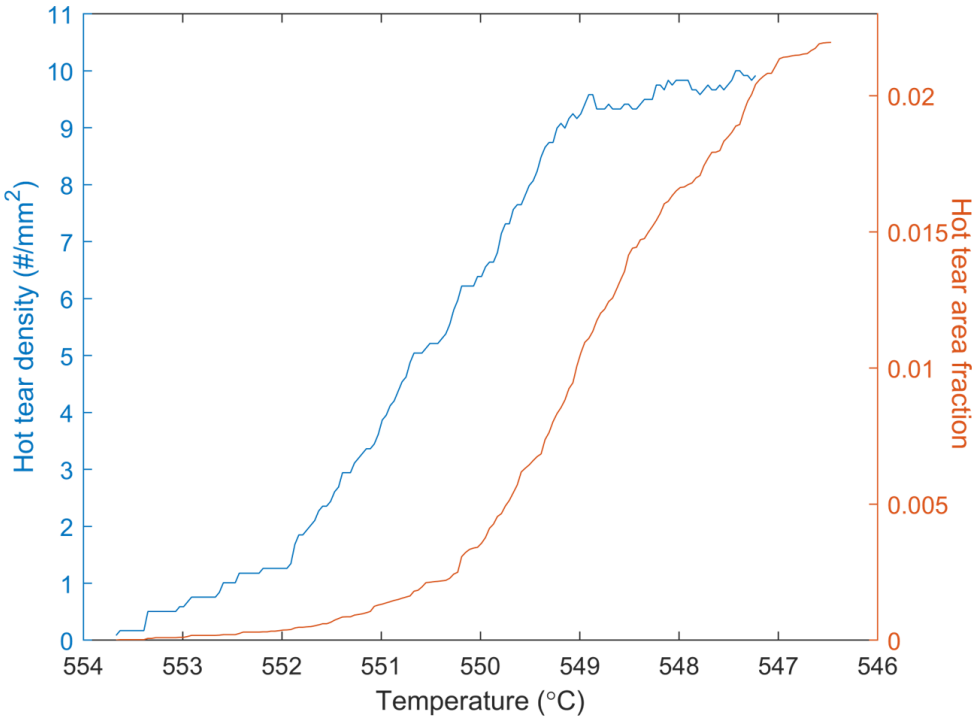

Figure 5. Hot tear density (blue) and area fraction (orange) as a function of temperature during the solidification of Al-5wt%Cu at a cooling rate of $2\,^{\circ}\mathrm{C\,s^{-1}}$

The hot tear detection algorithm was also used to investigate the sequence in which hot tears merged. For example, figure 6 shows a single, mm-scale hot tear that was formed by merging of thirty-six distinct and separate hot tears (each color indicates an originally independent hot tear). Although more data is required, one insight that the approach suggests – and which is unavailable from post-solidification analysis – is that large hot tears normally assumed to be a single tear may instead be due to the merging of a large number of smaller, initially separate tears.

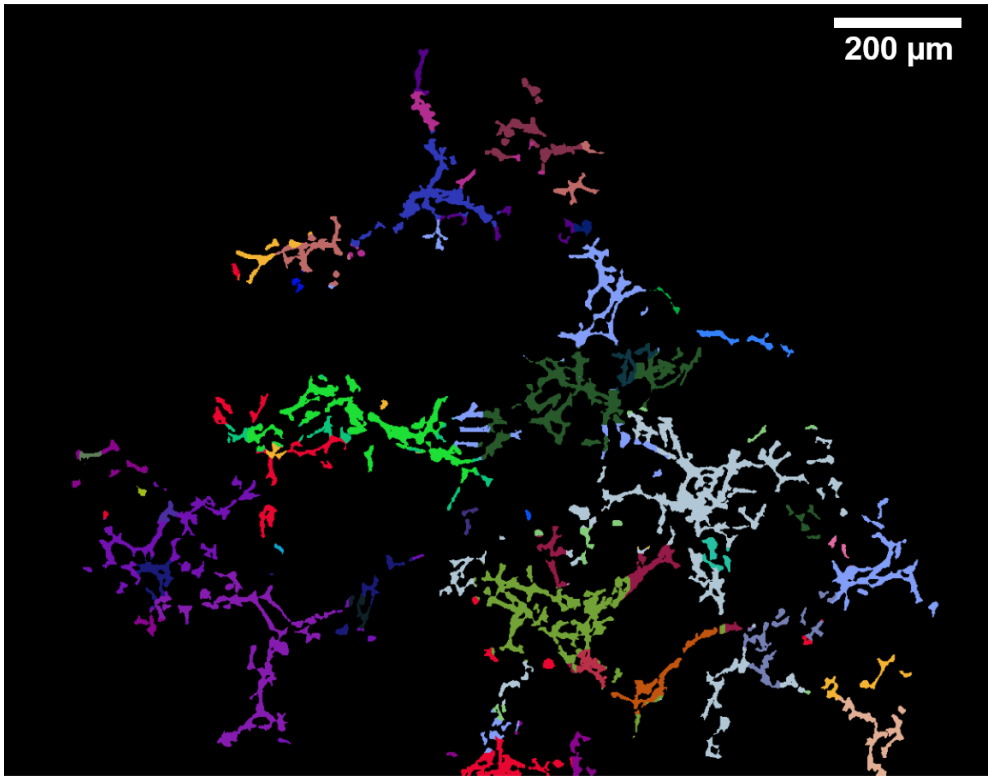

Figure 6. A large single inter-connected hot tear formed by the progressive merging of thirty-six initially separate (and differently coloured) tears, each with a different initial UI.

4. Conclusions

A novel algorithm was developed to extract quantified information of the evolution of hot tears from X-ray radiography video sequences of the solidification of metal alloys. The capabilities have been demonstrated using video sequences of a solidifying Al-5wt%Cu alloy. The algorithm allowed for the measurement of the formation and growth of hot tears for an ensemble of hot tears, each tracked in detail, and including analysis of interactions between existing hot tears such as merging. Further work is underway to extend the analysis to other fast X-ray radiography video sequences of other alloys with different solidification sequences, to give more robust insights into phenomena controlling hot tearing. We are also considering the development of algorithms for 3D analysis of high speed synchrotron tomographic sequences to overcome the constrains arising with thin samples. Continuing efforts that combine X-ray imaging experiments and automated computational analyses will likely help researchers decipher further the complexities of defect formation and solidification phenomena.

Acknowledgments

The work was funded by EPSRC (UK) under grant number EP/N007638/1 (Future Liquid Metal Engineering Hub). The synchrotron work was enabled by beamtime I-20210153 EC at the Petra III (Desy) beamline (Germany).

References

[1] Campbell J 2015 *Complete casting handbook: metal casting processes, metallurgy, techniques and design* (Butterworth-Heinemann)

[2] Eskin D, Katgerman L *et al.* 2004 *Progress in Materials Science* **49** 629–711

[3] Zhang J and Singer R 2002 *Acta Materialia* **50** 1869–1879

[4] Easton M, Wang H, Grandfield J, St John D and Sweet E 2004 *Materials Forum* vol 28 pp 224–229

[5] Cao G P and Kou S D 2006 *Metallurgical and Materials Transactions A* **37** 3647–3663

[6] Farup I, Drezet J M and Rappaz M 2001 *Acta Materialia* **49** 1261–1269

[7] Davidson C, Viano D, Lu L and StJohn D 2006 *International Journal of Cast Metals Research* **19** 59–65

[8] Sistaninia M, Terzi S, Phillion A, Drezet J M and Rappaz M 2013 *Acta Materialia* **61** 3831–3841

[9] Puncreobutr C, Phillion A, Fife J and Lee P 2014 *Acta Materialia* **64** 316–325

[10] Feng S, Han I, Lui A, Vincent R, Ring G, Grant P S and Liotti E 2022 *Metals* **12** 395

[11] Liotti E, Lui A, Connolley T and Grant P S 2022 *Acta Materialia* **240** 118298